FERMILAB-PUB-11-246-E-PPD

Measurements of inclusive W+jets production rates as a function of jet transverse momentum in $p\bar{p}$ collisions at $\sqrt{s} = 1.96$ TeV

V.M. Abazov,[35] B. Abbott,[73] B.S. Acharya,[29] M. Adams,[49] T. Adams,[47] G.D. Alexeev,[35] G. Alkhazov,[39] A. Alton[a],[61] G. Alverson,[60] G.A. Alves,[2] M. Aoki,[48] M. Arov,[58] A. Askew,[47] B. Åsman,[41] O. Atramentov,[65] C. Avila,[8] J. BackusMayes,[80] F. Badaud,[13] L. Bagby,[48] B. Baldin,[48] D.V. Bandurin,[47] S. Banerjee,[29] E. Barberis,[60] P. Baringer,[56] J. Barreto,[3] J.F. Bartlett,[48] U. Bassler,[18] V. Bazterra,[49] S. Beale,[6] A. Bean,[56] M. Begalli,[3] M. Begel,[71] C. Belanger-Champagne,[41] L. Bellantoni,[48] S.B. Beri,[27] G. Bernardi,[17] R. Bernhard,[22] I. Bertram,[42] M. Besançon,[18] R. Beuselinck,[43] V.A. Bezzubov,[38] P.C. Bhat,[48] V. Bhatnagar,[27] G. Blazey,[50] S. Blessing,[47] K. Bloom,[64] A. Boehnlein,[48] D. Boline,[70] E.E. Boos,[37] G. Borissov,[42] T. Bose,[59] A. Brandt,[76] O. Brandt,[23] R. Brock,[62] G. Brooijmans,[68] A. Bross,[48] D. Brown,[17] J. Brown,[17] X.B. Bu,[48] M. Buehler,[79] V. Buescher,[24] V. Bunichev,[37] S. Burdin[b],[42] T.H. Burnett,[80] C.P. Buszello,[41] B. Calpas,[15] E. Camacho-Pérez,[32] M.A. Carrasco-Lizarraga,[56] B.C.K. Casey,[48] H. Castilla-Valdez,[32] S. Chakrabarti,[70] D. Chakraborty,[50] K.M. Chan,[54] A. Chandra,[78] G. Chen,[56] S. Chevalier-Théry,[18] D.K. Cho,[75] S.W. Cho,[31] S. Choi,[31] B. Choudhary,[28] S. Cihangir,[48] D. Claes,[64] J. Clutter,[56] M. Cooke,[48] W.E. Cooper,[48] M. Corcoran,[78] F. Couderc,[18] M.-C. Cousinou,[15] A. Croc,[18] D. Cutts,[75] A. Das,[45] G. Davies,[43] K. De,[76] S.J. de Jong,[34] E. De La Cruz-Burelo,[32] F. Déliot,[18] M. Demarteau,[48] R. Demina,[69] D. Denisov,[48] S.P. Denisov,[38] S. Desai,[48] C. Deterre,[18] K. DeVaughan,[64] H.T. Diehl,[48] M. Diesburg,[48] P.F. Ding,[44] A. Dominguez,[64] T. Dorland,[80] A. Dubey,[28] L.V. Dudko,[37] D. Duggan,[65] A. Duperrin,[15] S. Dutt,[27] A. Dyshkant,[50] M. Eads,[64] D. Edmunds,[62] J. Ellison,[46] V.D. Elvira,[48] Y. Enari,[17] H. Evans,[52] A. Evdokimov,[71] V.N. Evdokimov,[38] G. Facini,[60] T. Ferbel,[69] F. Fiedler,[24] F. Filthaut,[34] W. Fisher,[62] H.E. Fisk,[48] M. Fortner,[50] H. Fox,[42] S. Fuess,[48] A. Garcia-Bellido,[69] V. Gavrilov,[36] P. Gay,[13] W. Geng,[15,62] D. Gerbaudo,[66] C.E. Gerber,[49] Y. Gershtein,[65] G. Ginther,[48,69] G. Golovanov,[35] A. Goussiou,[80] P.D. Grannis,[70] S. Greder,[19] H. Greenlee,[48] Z.D. Greenwood,[58] E.M. Gregores,[4] G. Grenier,[20] Ph. Gris,[13] J.-F. Grivaz,[16] A. Grohsjean,[18] S. Grünendahl,[48] M.W. Grünewald,[30] T. Guillemin,[16] F. Guo,[70] G. Gutierrez,[48] P. Gutierrez,[73] A. Haas[c],[68] S. Hagopian,[47] J. Haley,[60] L. Han,[7] K. Harder,[44] A. Harel,[69] J.M. Hauptman,[55] J. Hays,[43] T. Head,[44] T. Hebbeker,[21] D. Hedin,[50] H. Hegab,[74] A.P. Heinson,[46] U. Heintz,[75] C. Hensel,[23] I. Heredia-De La Cruz,[32] K. Herner,[61] G. Hesketh[d],[44] M.D. Hildreth,[54] R. Hirosky,[79] T. Hoang,[47] J.D. Hobbs,[70] B. Hoeneisen,[12] M. Hohlfeld,[24] Z. Hubacek,[10,18] N. Huske,[17] V. Hynek,[10] I. Iashvili,[67] Y. Ilchenko,[77] R. Illingworth,[48] A.S. Ito,[48] S. Jabeen,[75] M. Jaffré,[16] D. Jamin,[15] A. Jayasinghe,[73] R. Jesik,[43] K. Johns,[45] M. Johnson,[48] D. Johnston,[64] A. Jonckheere,[48] P. Jonsson,[43] J. Joshi,[27] A.W. Jung,[48] A. Juste,[40] K. Kaadze,[57] E. Kajfasz,[15] D. Karmanov,[37] P.A. Kasper,[48] I. Katsanos,[64] R. Kehoe,[77] S. Kermiche,[15] N. Khalatyan,[48] A. Khanov,[74] A. Kharchilava,[67] Y.N. Kharzheev,[35] M.H. Kirby,[51] J.M. Kohli,[27] A.V. Kozelov,[38] J. Kraus,[62] S. Kulikov,[38] A. Kumar,[67] A. Kupco,[11] T. Kurča,[20] V.A. Kuzmin,[37] J. Kvita,[9] S. Lammers,[52] G. Landsberg,[75] P. Lebrun,[20] H.S. Lee,[31] S.W. Lee,[55] W.M. Lee,[48] J. Lellouch,[17] L. Li,[46] Q.Z. Li,[48] S.M. Lietti,[5] J.K. Lim,[31] D. Lincoln,[48] J. Linnemann,[62] V.V. Lipaev,[38] R. Lipton,[48] Y. Liu,[7] Z. Liu,[6] A. Lobodenko,[39] M. Lokajicek,[11] R. Lopes de Sa,[70] H.J. Lubatti,[80] R. Luna-Garcia[e],[32] A.L. Lyon,[48] A.K.A. Maciel,[2] D. Mackin,[78] R. Madar,[18] R. Magaña-Villalba,[32] S. Malik,[64] V.L. Malyshev,[35] Y. Maravin,[57] J. Martínez-Ortega,[32] R. McCarthy,[70] C.L. McGivern,[56] M.M. Meijer,[34] A. Melnitchouk,[63] D. Menezes,[50] P.G. Mercadante,[4] M. Merkin,[37] A. Meyer,[21] J. Meyer,[23] F. Miconi,[19] N.K. Mondal,[29] G.S. Muanza,[15] M. Mulhearn,[79] E. Nagy,[15] M. Naimuddin,[28] M. Narain,[75] R. Nayyar,[28] H.A. Neal,[61] J.P. Negret,[8] P. Neustroev,[39] S.F. Novaes,[5] T. Nunnemann,[25] G. Obrant[‡],[39] J. Orduna,[78] N. Osman,[15] J. Osta,[54] G.J. Otero y Garzón,[1] M. Padilla,[46] A. Pal,[76] N. Parashar,[53] V. Parihar,[75] S.K. Park,[31] J. Parsons,[68] R. Partridge[c],[75] N. Parua,[52] A. Patwa,[71] B. Penning,[48] M. Perfilov,[37] K. Peters,[44] Y. Peters,[44] K. Petridis,[44] G. Petrillo,[69] P. Pétroff,[16] R. Piegaia,[1] M.-A. Pleier,[71] P.L.M. Podesta-Lerma[f],[32] V.M. Podstavkov,[48] P. Polozov,[36] A.V. Popov,[38] M. Prewitt,[78] D. Price,[52] N. Prokopenko,[38] S. Protopopescu,[71] J. Qian,[61] A. Quadt,[23] B. Quinn,[63] M.S. Rangel,[2] K. Ranjan,[28] P.N. Ratoff,[42] I. Razumov,[38] P. Renkel,[77] M. Rijssenbeek,[70] I. Ripp-Baudot,[19] F. Rizatdinova,[74] M. Rominsky,[48] A. Ross,[42] C. Royon,[18] P. Rubinov,[48] R. Ruchti,[54] G. Safronov,[36] G. Sajot,[14] P. Salcido,[50] A. Sánchez-Hernández,[32] M.P. Sanders,[25] B. Sanghi,[48] A.S. Santos,[5] G. Savage,[48] L. Sawyer,[58] T. Scanlon,[43] R.D. Schamberger,[70] Y. Scheglov,[39] H. Schellman,[51] T. Schliephake,[26] S. Schlobohm,[80] C. Schwanenberger,[44] R. Schwienhorst,[62] J. Sekaric,[56] H. Severini,[73] E. Shabalina,[23] V. Shary,[18] A.A. Shchukin,[38]

Operated by Fermi Research Alliance, LLC under Contract No. DE-AC02-07CH11359 with the United States Department of Energy.

R.K. Shivpuri,[28] V. Simak,[10] V. Sirotenko,[48] P. Skubic,[73] P. Slattery,[69] D. Smirnov,[54] K.J. Smith,[67] G.R. Snow,[64] J. Snow,[72] S. Snyder,[71] S. Söldner-Rembold,[44] L. Sonnenschein,[21] K. Soustruznik,[9] J. Stark,[14] V. Stolin,[36] D.A. Stoyanova,[38] M. Strauss,[73] D. Strom,[49] L. Stutte,[48] L. Suter,[44] P. Svoisky,[73] M. Takahashi,[44] A. Tanasijczuk,[1] W. Taylor,[6] M. Titov,[18] V.V. Tokmenin,[35] Y.-T. Tsai,[69] D. Tsybychev,[70] B. Tuchming,[18] C. Tully,[66] L. Uvarov,[39] S. Uvarov,[39] S. Uzunyan,[50] R. Van Kooten,[52] W.M. van Leeuwen,[33] N. Varelas,[49] E.W. Varnes,[45] I.A. Vasilyev,[38] P. Verdier,[20] L.S. Vertogradov,[35] M. Verzocchi,[48] M. Vesterinen,[44] D. Vilanova,[18] P. Vokac,[10] H.D. Wahl,[47] M.H.L.S. Wang,[48] J. Warchol,[54] G. Watts,[80] M. Wayne,[54] M. Weber[g],[48] L. Welty-Rieger,[51] A. White,[76] D. Wicke,[26] M.R.J. Williams,[42] G.W. Wilson,[56] M. Wobisch,[58] D.R. Wood,[60] T.R. Wyatt,[44] Y. Xie,[48] C. Xu,[61] S. Yacoob,[51] R. Yamada,[48] W.-C. Yang,[44] T. Yasuda,[48] Y.A. Yatsunenko,[35] Z. Ye,[48] H. Yin,[48] K. Yip,[71] S.W. Youn,[48] J. Yu,[76] S. Zelitch,[79] T. Zhao,[80] B. Zhou,[61] J. Zhu,[61] M. Zielinski,[69] D. Zieminska,[52] and L. Zivkovic[75]

(The D0 Collaboration*)

[1] *Universidad de Buenos Aires, Buenos Aires, Argentina*
[2] *LAFEX, Centro Brasileiro de Pesquisas Físicas, Rio de Janeiro, Brazil*
[3] *Universidade do Estado do Rio de Janeiro, Rio de Janeiro, Brazil*
[4] *Universidade Federal do ABC, Santo André, Brazil*
[5] *Instituto de Física Teórica, Universidade Estadual Paulista, São Paulo, Brazil*
[6] *Simon Fraser University, Vancouver, British Columbia, and York University, Toronto, Ontario, Canada*
[7] *University of Science and Technology of China, Hefei, People's Republic of China*
[8] *Universidad de los Andes, Bogotá, Colombia*
[9] *Charles University, Faculty of Mathematics and Physics, Center for Particle Physics, Prague, Czech Republic*
[10] *Czech Technical University in Prague, Prague, Czech Republic*
[11] *Center for Particle Physics, Institute of Physics, Academy of Sciences of the Czech Republic, Prague, Czech Republic*
[12] *Universidad San Francisco de Quito, Quito, Ecuador*
[13] *LPC, Université Blaise Pascal, CNRS/IN2P3, Clermont, France*
[14] *LPSC, Université Joseph Fourier Grenoble 1, CNRS/IN2P3, Institut National Polytechnique de Grenoble, Grenoble, France*
[15] *CPPM, Aix-Marseille Université, CNRS/IN2P3, Marseille, France*
[16] *LAL, Université Paris-Sud, CNRS/IN2P3, Orsay, France*
[17] *LPNHE, Universités Paris VI and VII, CNRS/IN2P3, Paris, France*
[18] *CEA, Irfu, SPP, Saclay, France*
[19] *IPHC, Université de Strasbourg, CNRS/IN2P3, Strasbourg, France*
[20] *IPNL, Université Lyon 1, CNRS/IN2P3, Villeurbanne, France and Université de Lyon, Lyon, France*
[21] *III. Physikalisches Institut A, RWTH Aachen University, Aachen, Germany*
[22] *Physikalisches Institut, Universität Freiburg, Freiburg, Germany*
[23] *II. Physikalisches Institut, Georg-August-Universität Göttingen, Göttingen, Germany*
[24] *Institut für Physik, Universität Mainz, Mainz, Germany*
[25] *Ludwig-Maximilians-Universität München, München, Germany*
[26] *Fachbereich Physik, Bergische Universität Wuppertal, Wuppertal, Germany*
[27] *Panjab University, Chandigarh, India*
[28] *Delhi University, Delhi, India*
[29] *Tata Institute of Fundamental Research, Mumbai, India*
[30] *University College Dublin, Dublin, Ireland*
[31] *Korea Detector Laboratory, Korea University, Seoul, Korea*
[32] *CINVESTAV, Mexico City, Mexico*
[33] *Nikhef, Science Park, Amsterdam, the Netherlands*
[34] *Radboud University Nijmegen, Nijmegen, the Netherlands and Nikhef, Science Park, Amsterdam, the Netherlands*
[35] *Joint Institute for Nuclear Research, Dubna, Russia*
[36] *Institute for Theoretical and Experimental Physics, Moscow, Russia*
[37] *Moscow State University, Moscow, Russia*
[38] *Institute for High Energy Physics, Protvino, Russia*
[39] *Petersburg Nuclear Physics Institute, St. Petersburg, Russia*
[40] *Institució Catalana de Recerca i Estudis Avançats (ICREA) and Institut de Física d'Altes Energies (IFAE), Barcelona, Spain*
[41] *Stockholm University, Stockholm and Uppsala University, Uppsala, Sweden*
[42] *Lancaster University, Lancaster LA1 4YB, United Kingdom*
[43] *Imperial College London, London SW7 2AZ, United Kingdom*
[44] *The University of Manchester, Manchester M13 9PL, United Kingdom*
[45] *University of Arizona, Tucson, Arizona 85721, USA*
[46] *University of California Riverside, Riverside, California 92521, USA*
[47] *Florida State University, Tallahassee, Florida 32306, USA*

[48]Fermi National Accelerator Laboratory, Batavia, Illinois 60510, USA
[49]University of Illinois at Chicago, Chicago, Illinois 60607, USA
[50]Northern Illinois University, DeKalb, Illinois 60115, USA
[51]Northwestern University, Evanston, Illinois 60208, USA
[52]Indiana University, Bloomington, Indiana 47405, USA
[53]Purdue University Calumet, Hammond, Indiana 46323, USA
[54]University of Notre Dame, Notre Dame, Indiana 46556, USA
[55]Iowa State University, Ames, Iowa 50011, USA
[56]University of Kansas, Lawrence, Kansas 66045, USA
[57]Kansas State University, Manhattan, Kansas 66506, USA
[58]Louisiana Tech University, Ruston, Louisiana 71272, USA
[59]Boston University, Boston, Massachusetts 02215, USA
[60]Northeastern University, Boston, Massachusetts 02115, USA
[61]University of Michigan, Ann Arbor, Michigan 48109, USA
[62]Michigan State University, East Lansing, Michigan 48824, USA
[63]University of Mississippi, University, Mississippi 38677, USA
[64]University of Nebraska, Lincoln, Nebraska 68588, USA
[65]Rutgers University, Piscataway, New Jersey 08855, USA
[66]Princeton University, Princeton, New Jersey 08544, USA
[67]State University of New York, Buffalo, New York 14260, USA
[68]Columbia University, New York, New York 10027, USA
[69]University of Rochester, Rochester, New York 14627, USA
[70]State University of New York, Stony Brook, New York 11794, USA
[71]Brookhaven National Laboratory, Upton, New York 11973, USA
[72]Langston University, Langston, Oklahoma 73050, USA
[73]University of Oklahoma, Norman, Oklahoma 73019, USA
[74]Oklahoma State University, Stillwater, Oklahoma 74078, USA
[75]Brown University, Providence, Rhode Island 02912, USA
[76]University of Texas, Arlington, Texas 76019, USA
[77]Southern Methodist University, Dallas, Texas 75275, USA
[78]Rice University, Houston, Texas 77005, USA
[79]University of Virginia, Charlottesville, Virginia 22901, USA
[80]University of Washington, Seattle, Washington 98195, USA

(Dated: June 7, 2011)

This Letter describes measurements of inclusive $W(\to e\nu) + n$ jet cross sections (n =1–4), presented as total inclusive cross sections and differentially in the n^{th} jet transverse momentum. The measurements are made using data corresponding to an integrated luminosity of 4.2 fb^{-1} collected by the D0 detector at the Fermilab Tevatron Collider, and achieve considerably smaller uncertainties on W+jets production cross sections than previous measurements. The measurements are compared to next-to-leading order perturbative QCD (pQCD) calculations in the n =1–3 jet multiplicity bins and to leading order pQCD calculations in the 4-jet bin. The measurements are generally in agreement with pQCD predictions, although certain regions of phase space are identified where the calculations could be improved.

PACS numbers: 12.38.Bx, 13.85.Qk, 14.70.Fm

Measurements of vector boson plus jet production are fundamental tests of perturbative quantum chromodynamics (pQCD), the theory describing the strong interaction. In addition to providing a test of pQCD at high momentum scales, W+jets production can be the dominant background in measurements of single top quark and $t\bar{t}$ production as well as in searches for the standard model Higgs boson and for physics beyond the standard model. Theoretical uncertainties on the production rates and kinematics introduce limitations in our ability to identify new physics signals. Therefore, it is crucial to make precision measurements of W+jets production at the Fermilab Tevatron Collider and the CERN Large Hadron Collider in order to constrain these backgrounds. We present new measurements of W+jets cross sections with a data sample more than ten times larger than that used in previous measurements [1], allowing the first detailed study of $W + 4$ jet production. The previous measurements have been used extensively in testing and tuning theoretical models of W boson production [2–4].

The strategy employed for this measurement is based on those used in the D0 Z+jet cross section [5] and Z boson p_T [6] publications. We select a high purity sample of W+jets events, without introducing any bias in the selection that would result in different efficiencies depending on the jet kinematics of the final state. The results are corrected to the "particle level," which includes energy from stable particles, the underlying event, muons, and

*with visitors from [a]Augustana College, Sioux Falls, SD, USA, [b]The University of Liverpool, Liverpool, UK, [c]SLAC, Menlo Park, CA, USA, [d]University College London, London, UK, [e]Centro de Investigacion en Computacion - IPN, Mexico City, Mexico,

neutrinos, as defined in Ref. [7]. This procedure corrects a measured observable back to the particle level observable, correcting for the effect of finite experimental resolution, detector response, acceptance, and efficiencies.

These measurements use a sample of $W(\to e\nu) + n$ jet candidate events corresponding to an integrated luminosity of 4.2 fb^{-1} collected with the D0 detector in Run II of the Fermilab Tevatron Collider. The D0 detector consists of a central tracking system, comprising a silicon microstrip tracker and a fiber tracker, both within an approximately 2 T axial magnetic field. These components are used primarily to identify the location of the $p\bar{p}$ interaction vertex and the electron produced in the decay of the W boson candidate. Outside of the tracking system, a liquid-argon and uranium calorimeter is divided into a central section and two end sections that are used to identify electromagnetic and hadronic showers. A detailed description of the D0 detector can be found in Ref. [8].

The data were collected using a suite of electron and electron+jet triggers. The events were then processed through the D0 reconstruction program which identifies jet and W boson candidates. Jets are identified with the D0 midpoint cone algorithm [9], which uses a cone of radius $\mathcal{R} = 0.5$ to cluster calorimeter cells. Jets are corrected for the calorimeter response, instrumental and out-of-cone showering effects, and additional energy deposits in the calorimeter that arise from detector noise and pile-up from multiple interactions and different beam crossings. These jet energy scale corrections are determined using transverse momentum imbalance in γ + jet events, where the electromagnetic calorimeter response is calibrated using $Z/\gamma^* \to e^+e^-$ events. Jets are required to have at least two tracks that point to their associated $p\bar{p}$ vertex. Jets are ordered in decreasing transverse momentum and we call the jet with the highest transverse momentum "leading." Electrons are identified as clusters of calorimeter cells in which 95% of the energy in the shower is deposited in the electromagnetic (EM) section. The electron candidates must be isolated from other calorimeter energy deposits, have spatial distributions consistent with those expected for electron showers, and the event must contain a reconstructed track matched to the EM shower that is isolated from other tracks. Events with a second isolated electron are removed to suppress the background from Z boson and Drell-Yan production. The missing transverse energy $\not\!\!E_T$ in the event is calculated as a vector sum of the calorimeter cell energies and is corrected for the presence of any muons. Because the longitudinal component of the momentum of the neutrino is not measured, the measured properties of the W boson candidates are limited to their transverse energy, E_T^W, and transverse mass, defined as

$$M_T^W = \sqrt{(\not\!\!E_T + p_T^e)^2 - (\not\!\!E_x + p_x^e)^2 - (\not\!\!E_y + p_y^e)^2} \quad (1)$$

where p_T^e is the transverse momentum of the electron, and p_x^e and p_y^e are the x and y components of the electron's momentum [10].

The following event selections are used in order to suppress background while maintaining high efficiency for events in which a W boson was produced: $p_T^e \geq 15$ GeV and electron pseudorapidity $|\eta^e| < 1.1$, $\not\!\!E_T > 20$ GeV, $M_T^W \geq 40$ GeV, jet transverse momentum $p_T^{\rm jet} \geq 20$ GeV and rapidity $|y^{\rm jet}| < 3.2$, $\Delta\mathcal{R} = \sqrt{(\Delta\phi)^2 + (\Delta\eta)^2}$ between the electron and the nearest jet > 0.5, and the z component of the $p\bar{p}$ interaction vertex is restricted to $|z_{\rm vtx}| < 60$ cm [10]. Events must have a reconstructed $p\bar{p}$ interaction vertex, containing at least three associated tracks. This $p\bar{p}$ interaction vertex is required to be less than 1 cm away in the coordinate along the beam line from the extrapolated electron track.

After these requirements, W(+jets) events dominate the data sample but there are backgrounds from Z+jets, $t\bar{t}$, diboson, single top quarks, and multijet events. We simulate the W/Z+jets and $t\bar{t}$ processes with ALPGEN [11] interfaced with PYTHIA [12] for the simulation of initial and final state radiation and for parton hadronization. The PYTHIA generator is used to simulate diboson production, while production of single top quarks is simulated with the COMPHEP [13] generator interfaced with PYTHIA. The cross sections for W/Z+jet production are taken from ALPGEN, corrected with a constant multiplicative factor to match the inclusive W/Z+jet cross sections calculated at NLO [14]. Additional corrections are applied to events containing W/Z bosons plus heavy flavor jets, to match the predictions of NLO QCD calculations. Events from randomly chosen beam crossings, with the same instantaneous luminosity profile as the data, are overlaid on the simulated events to reproduce the effect of multiple $p\bar{p}$ interactions and detector noise. All simulated samples are passed through the D0 detector simulation and then reconstructed in the same way as the data. The estimated fraction of the data sample that is due to processes other than W+jets ranges within (2–40)%, and the fraction of background due to top quark production ranges within (0–20)%, with the larger contributions at higher jet multiplicities in both cases.

In multijet events, there is a small but non-negligible chance that a jet may be misidentified as an electron and then the event may pass all selection criteria. As the multijet cross section is large, the contribution from such instances of fake-electron events to the measured distributions must be taken into account. To determine the number and kinematic distributions of such events, we use the data-driven method described in Ref. [15]. This approach uses data in a control region that has no overlap with the signal selection to determine the differential distribution and overall normalization of the multijet distributions, because the estimation of this background from

Monte Carlo simulations is not reliable.

The total background contribution is subtracted from the data in each bin of the $p_T^{\rm jet}$ distribution. After background subtraction, the data are corrected for detector resolution effects using a regularized inversion of the resolution matrix as implemented in the program GURU [16], with ensemble testing used to derive statistical uncertainties and unfolding biases. This method is described in detail in Ref. [6]. We have chosen the matrix unfolding approach over the traditional bin-by-bin correction method because of non-negligible bin migration effects in the $p_T^{\rm jet}$ variable and because the matrix unfolding method provides improved estimation of the uncertainties of the measurement.

To evaluate statistical uncertainties on the unfolded distributions, as well as systematic biases and uncertainties, we build ensembles using ALPGEN+PYTHIA events that have the same statistical fluctuations as the data sample. The ensembles are reweighted to accurately describe the kinematics of the unfolded jet p_T. Five hundred ensembles are created and unfolded in the same manner as the data and are in-turn compared to their corresponding generator-level distributions. The residual differences between the generator-level and unfolded measurement in each bin, for each ensemble, are determined and fitted with a Gaussian function. The mean offset of the distribution is used to construct an unfolding bias correction to be applied to the data, while the larger of the root mean square and the Gaussian width is assigned as the statistical uncertainty associated with that bin in the unfolded distribution. The unfolding bias correction is small, generally (0.5–2)%, and always much smaller than the statistical uncertainty in the bin. Overall, the statistical uncertainties are within (1–17)%, depending on jet multiplicity and jet p_T bin.

The systematic uncertainties affecting this measurement can be divided into two types: those related to the knowledge of the detector response and those related to the background modeling and unfolding method. The systematic uncertainties related to the modeling of the detector response and their effect on the final cross sections arise from the calibration of the jet energy scale [(3–16)%], from the measurements of the jet energy resolution [(0.1–17)%], the jet identification efficiency [(0.3–4)%], the jet-track matching requirement [(1–11)%], the trigger efficiency [(1–4)%], the electron identification efficiency [(4–5)%], and the uncertainty in the luminosity determination (6.1%).

All differential cross sections measurements are normalized to the measured inclusive W boson cross section, resulting in a complete (partial) cancellation of the systematic uncertainties due to luminosity (trigger and electron identification efficiencies). The remaining sources of systematic uncertainty are the normalization and differential distributions of the multijet background [(0.1–4)%], the theoretical uncertainty on the $t\bar{t}$ cross section [(0–19)%], the uncertainty due to the electron final state radiation at particle level (<1%), and uncertainties associated with the unfolding method (<1%).

As in the case of the differential cross section measurements, the inclusive $W(\rightarrow e\nu)$+jets production cross sections are normalized to the measured inclusive $W \rightarrow e\nu$ cross section. This normalization reduces (or cancels) systematic uncertainties and provides sensitivity to the shape of the distribution in comparisons to Monte Carlo and theoretical predictions. The events passing the selection requirements are well described by the Monte Carlo predictions and the sample is dominated ($> 99.8\%$) by the inclusive production of W events. The total inclusive W boson cross section within the kinematic acceptance is measured to be $\sigma_W = 1132 \pm 1(\text{stat})\ ^{+43}_{-84}(\text{syst}) \pm 69(\text{lumi})$ pb. This number is used to normalize the differential cross section results.

Recent theoretical work [3, 17] has extended the availability of predictions up to W+3 jet events at NLO. Although there has also been a recent calculation of W+4 jet production at NLO for pp collisions at $\sqrt{s} = 7$ (or 14) TeV [18], these predictions are not available for the Tevatron, and comparisons with theory are therefore limited to LO for W+4 jet production. In this analysis, we use the interfaced BLACKHAT+SHERPA [19] and ROCKET+MCFM [20, 21] programs as the main sources for theoretical predictions of W+jets production. BLACKHAT and ROCKET are parton level generators which incorporate NLO QCD calculations with up to 3 final state partons interfaced to parton shower programs which provide parton level jets corresponding to the hard partons, but do not include the underlying event or hadronization effects. We compare both theory predictions to our measured cross sections, in order to determine the differences that arise from theoretical choices made in the calculations, such as the choice of renormalization and factorization scales, and in order to explore the uncertainties inherent in these predictions.

The BLACKHAT+SHERPA program employs the renormalization (μ_R) and factorization (μ_F) scale $\mu = \mu_F = \mu_R = \frac{1}{2}\hat{H}_T$, where $\hat{H}_T$ is the scalar sum of the parton and lepton transverse energies. BLACKHAT+SHERPA does not provide cross sections using the D0 midpoint jet algorithm, but instead uses the SISCONE [22] algorithm with split-merge parameter $f = 0.5$ and cone radius $\mathcal{R} = 0.5$. In order to keep all the theory predictions on the same footing, we therefore show the BLACKHAT+SHERPA and ROCKET+MCFM predictions using the SISCONE jet algorithm. However, we expect differences between the jet algorithms to be a negligible effect. The choice made by the ROCKET+MCFM authors is $\mu = \sqrt{M_W^2 + \frac{1}{4}(\Sigma p^{\rm jet})^2}$ (in the 2, 3, and 4-jet bins), summing over the four-momenta of jets in the event and M_W is the mass of the W boson. This scale choice was suggested in Ref. [23] because it sums large logarithms in the calculation to

all orders. In the 1-jet bin, a slightly modified choice of $\mu = \sqrt{M_W^2 + (p_T^{\rm jet})^2}$ is used. This is due to the fact that in the 1-jet bin, the NLO calculation includes diagrams with an extra hard (real) emission or virtual loop corrections. For the Born and virtual loop diagrams, the only hard scale is M_W, due to the single massless jet balancing the W boson. However, in the case of diagrams with an extra hard emission, the two final state partons can be combined into one massive jet by the jet reconstruction algorithm increasing the scale of the real contributions, which generally contribute positively to the cross section. As a result, the real diagrams are evaluated with a coupling that is smaller, due to the running of α_s, than the virtual diagrams, which leads to a prediction of the NLO cross section that is too low. Both theory calculations use the MSTW2008 parton density function (PDF) [24], where the LO (NLO) cross section calculation is matched to the LO (NLO) PDF. The uncertainties on the theory predictions are estimated by multiplying μ by factors of 2 and 0.5.

Fixed-order pQCD predictions provide only a parton-level prediction which is not immediately comparable to the unfolded data. Additional corrections must be applied to propagate the fixed order predictions to the particle level. The two effects which contribute to this parton-to-particle correction are hadronization of the final state partons and the presence of the underlying event. These corrections (referred to collectively as hadronization corrections) are obtained with the SHERPA MC program [4], which employs the CTEQ6.6 PDF set [25]. The corrections are generally around 10%, but are as large as 25% in the highest $p_T^{\rm jet}$ bins, due to the underlying event contribution. The parton level cross sections are computed with the SISCONE jet finding algorithm, while the particle level predictions are computed with the D0 midpoint cone algorithm, in order to account for the difference in jet algorithm between the data and the pQCD predictions. The impact of folding the correction for the jet algorithm into the overall hadronization correction is small, and well within the theoretical scale uncertainties. All inclusive and differential pQCD predictions have the hadronization corrections applied to them. We provide the tables of the hadronization corrections [26] so that future pQCD calculations can be compared to the data on the same terms.

Figure 1(a) shows the absolute inclusive $W + n$ jet cross sections for each jet multiplicity considered, compared with the LO and NLO theoretical predictions from BLACKHAT+SHERPA and ROCKET+MCFM. Figure 1(b) shows the ratio of theory to data. Good agreement is observed between data and the NLO theory predictions, except for the 1-jet bin, where the NLO prediction presents a slight excess with respect to the data. Figure 1(c) shows the measurement of the σ_n/σ_{n-1} inclusive cross section ratio as a function of inclusive jet multiplicity for

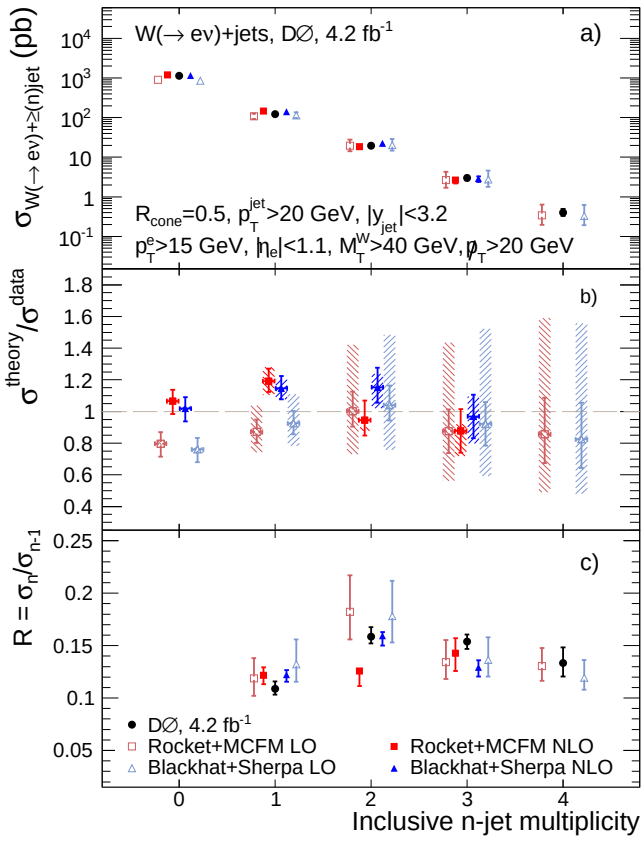

FIG. 1: (a) Total inclusive n-jet cross sections $\sigma_n = \sigma(W(\to e\nu) + \geq n$ jet; $p_T^{\rm jet} > 20$ GeV) as a function of inclusive jet multiplicity, (b) the ratio of the theory predictions to the measurements, and (c) σ_n/σ_{n-1} ratios for data, BLACKHAT+SHERPA and ROCKET+MCFM. Error bars on data points represent combined statistical and systematic uncertainties on measured cross sections. The hashed areas represent the theoretical uncertainty arising from the choice of renormalization and factorization scale.

n=1–4 in comparison to predictions of this ratio from LO and NLO calculations. Here, the theoretical uncertainty takes the correlations of the scale choice between the n and $n-1$ multiplicity bins into account. The data uncertainties are also calculated from the relative uncertainties on the two cross sections, but with partial or total cancellation of systematic uncertainties due to electron identification, trigger, and luminosity. The uncertainties due to the jet corrections are correlated between bins and are accounted for. The total uncertainties on the measurement presented throughout this paper are comparable to the scale uncertainties on the predictions at NLO. Tables of the measured and theoretical cross sections and their uncertainties are given in [26].

The differential data cross sections (multiplied by the branching fraction of the $W \to e\nu$ decay) for each jet multiplicity are shown in Figure 2. The data are normalized by the inclusive W cross section in all jet multiplicity

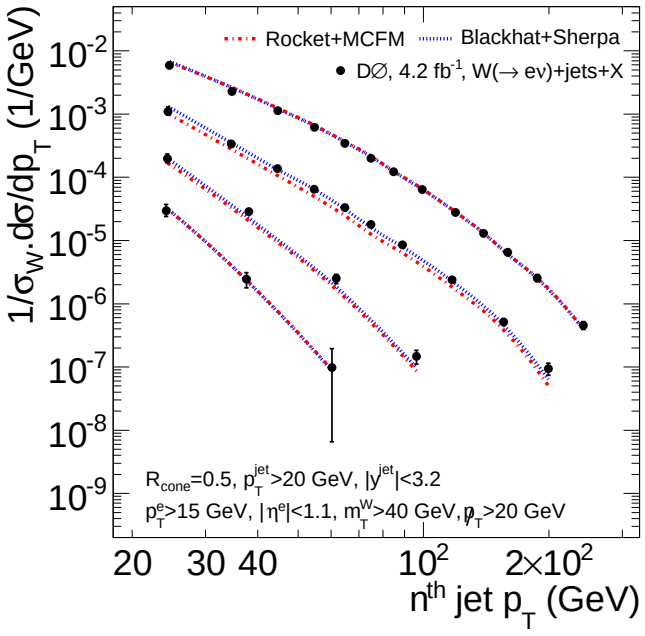

FIG. 2: Measured W+n jet differential cross section as a function of jet p_T for jet multiplicities n =1–4, normalized to the inclusive $W \to e\nu$ cross section. W+1 jet inclusive spectra are shown by the top curve, the W+4 jet inclusive spectra by the bottom curve. The measurements are compared to the fixed-order NLO predictions for the jet multiplicities n =1–3, and to LO predictions for $n = 4$.

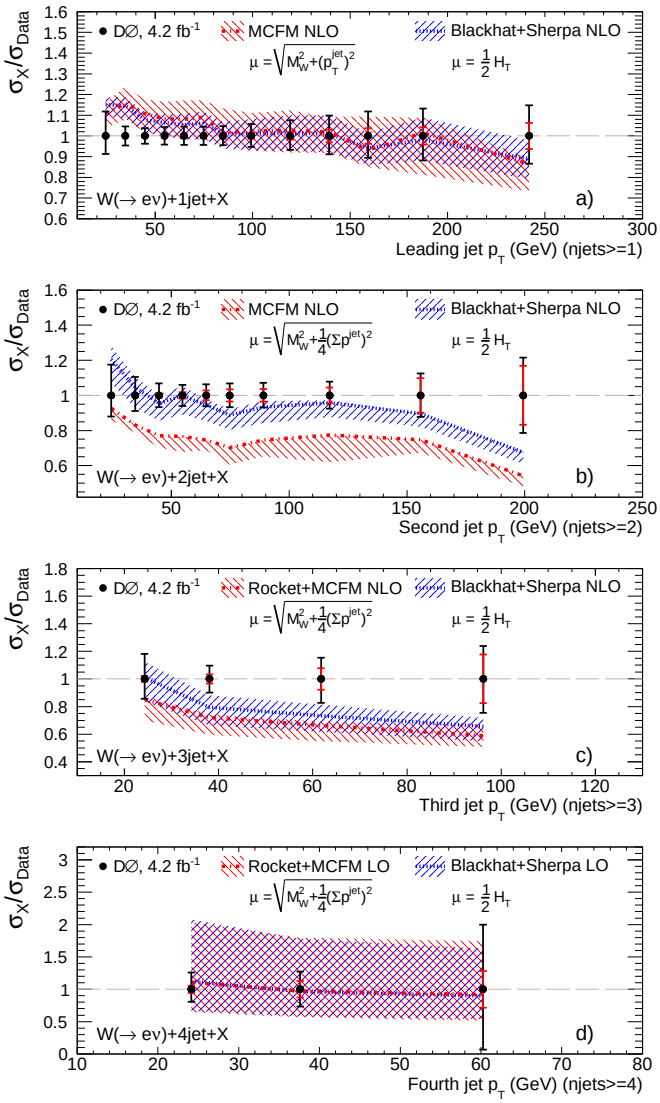

FIG. 3: The ratio of pQCD predictions to the measured differential cross sections for the n^{th} jet p_T in (a) W+1 jet events, (b) W+2 jet events, (c) W+3 jet events, and (d) W+4 jet events. The inner (red) bars represent the statistical uncertainties of the measurement, while the outer (black) bars represent the statistical and systematic uncertainties added in quadrature. The shaded areas indicate the theoretical uncertainties due to variations of the factorization and renormalization scale.

bins, which reduces the uncertainties in the measurement because of cancellation of some systematic uncertainties. The data spectra are compared to the predictions from ROCKET+MCFM and BLACKHAT+SHERPA (again normalized by their respective inclusive W cross sections). The theory is able to describe the data throughout the p_T^{jet} spectra for all multiplicities, although a detailed comparison is best made by examining the ratios of theory to data. The data are plotted at the average p_T^{jet} value for the events in each bin.

The ratio of the theory predictions to the unfolded differential data cross sections are shown in Figure 3. Each of the data and theory cross sections is normalized to its respective inclusive W boson production cross section. In the inclusive W+1 jet bin [Figure 3(a)], the data uncertainties vary by (4–14)%, but for most jet transverse momenta these uncertainties are smaller than the theoretical uncertainties. The data agree well with both NLO theory calculations, although the theoretical prediction is slightly higher than the data at low p_T^{jet}. The inclusive W+2 jet bin results are shown in Figure 3(b). The measured uncertainties vary by (5–20)% and are similar to those of the 1-jet bin. The BLACKHAT+SHERPA predictions are in good agreement with the data everywhere except at the smallest and highest values of p_T^{jet}. The MCFM predictions are significantly below the data. The difference between the two NLO calculations in this W+2 jet sample indicates that the scale uncertainties are larger than is indicated by the variation in μ by the conventional choice of 0.5 and 2. Also, the one-sided uncertainty band on the MCFM prediction indicates that the dependence of the cross section on μ has a local maximum at the particular choice of μ made here. In Figure 3(c), the ratio of W+3 jet pQCD predictions to the differential cross sections are shown. The results of NLO calculations are smaller than the measurement but still consistent within

uncertainties. In Figure 3(d), the differential cross section measurement of W+4 jets is shown as a ratio to the LO pQCD prediction. The theory prediction can reproduce the data, albeit with large uncertainties. An NLO prediction for this final state is necessary to make a more robust comparison.

In summary, W+n jet inclusive cross sections for $n = 1, 2, 3$ and 4 jets have been measured using 4.2 fb^{-1} of integrated luminosity collected by the D0 detector. The measurements include the total inclusive cross section for each jet multiplicity and differential cross sections as a function of the n^{th} jet p_T. These measurements represent a test of pQCD complementary to the extensive D0 Z+jets measurements [5, 27, 28]. The measured cross sections improve on the current measurement [1] by including W+4 jet differential cross sections, by significantly improving the uncertainties on differential cross sections in all jet multiplicities, and by performing the first comparison with NLO W+3 jet cross section predictions. The measured cross sections are generally found to agree with the NLO calculation although certain regions of phase space are identified where the calculations could be improved.

We thank the staffs at Fermilab and collaborating institutions, and acknowledge support from the DOE and NSF (USA); CEA and CNRS/IN2P3 (France); FASI, Rosatom and RFBR (Russia); CNPq, FAPERJ, FAPESP and FUNDUNESP (Brazil); DAE and DST (India); Colciencias (Colombia); CONACyT (Mexico); KRF and KOSEF (Korea); CONICET and UBACyT (Argentina); FOM (The Netherlands); STFC and the Royal Society (United Kingdom); MSMT and GACR (Czech Republic); CRC Program and NSERC (Canada); BMBF and DFG (Germany); SFI (Ireland); The Swedish Research Council (Sweden); and CAS and CNSF (China). The authors especially thank the ROCKET+MCFM and BLACKHAT+SHERPA authors for generating the theoretical predictions. We also especially thank Jan Winter for help with generating the hadronization corrections. Many thanks go to Giulia Zanderighi, Lance Dixon, Zvi Bern and Jan Winter for useful discussions.

[1] T. Aaltonen *et al.* [CDF Collaboration], Phys. Rev. D **77**, 011108 (2008).
[2] C. F. Berger *et al.*, Phys. Rev. D **80**, 074036 (2009).
[3] R. K. Ellis, K. Melnikov, and G. Zanderighi, Phys. Rev. D **80**, 094002 (2009).
[4] T. Gleisberg *et al.*, J. High Energy Phys. **02**, 007 (2009).
[5] V. M. Abazov *et al.* [D0 Collaboration], Phys. Lett. B **669**, 278 (2008).
[6] V. M. Abazov *et al.* [D0 Collaboration], Phys. Lett. B **693**, 522 (2010).
[7] C. Buttar *et al.*, arXiv:0803.0678 [hep-ph], Section 9.
[8] V. M. Abazov *et al.* [D0 Collaboration], Nucl. Instrum. Methods Phys. Res. A **565**, 463 (2006).
[9] G. C. Blazey *et al.*, Fermilab-Pub-00/297 (2000).
[10] We use a standard right-handed coordinate system. The nominal collision point is the center of the detector with coordinate $(0, 0, 0)$. The direction of the proton beam is the positive $+z$ axis. The $+x$ axis is horizontal, pointing away from the center of the Tevatron ring. The $+y$ axis points vertically upwards. The polar angle, θ, is defined such that $\theta = 0$ is the $+z$ direction. The rapidity is defined as $y = -\ln[(E + p_Z)/(E - p_Z)]$, where E is the energy and p_Z is the momentum component along the proton beam direction. Pseudorapidity is defined as $\eta = -\ln[\tan\frac{\theta}{2}]$. ϕ is defined as the azimuthal angle in the plane transverse to the proton beam direction.
[11] M. L. Mangano *et al.*, J. High Energy Phys. **07**, 001 (2003). We use version 2.11.
[12] T. Sjöstrand *et al.*, Comput. Phys. Commun. **135**, 238 (2001). We use version 6.403.
[13] E. Boos *et al.* [CompHEP Collaboration], Nucl. Instrum. Meth. Phys Res. A **534**, 250 (2004).
[14] J. Campbell and R.K. Ellis, Phys. Rev. D **65**, 113007 (2002); J. Campbell, R.K. Ellis, and D. Rainwater, Phys. Rev. D **68**, 094021 (2003).
[15] V. M. Abazov *et al.* [D0 Collaboration], Phys. Rev. D **76**, 092007 (2007).
[16] A. Hocker and V. Kartvelishvili, Nucl. Instrum. Meth. Phys. Res. A **372** (1996).
[17] C. F. Berger *et al.*, Phys. Rev. Lett. **102**, 222001 (2009).
[18] C. F. Berger *et al.*, Phys. Rev. Lett. **106**, 092001 (2011).
[19] C. F. Berger *et al.*, arXiv:0905.2735 [hep-ph].
[20] R. K. Ellis *et al.*, J. High Energy Phys. **01**, 012 (2009).
[21] W. T. Giele and G. Zanderighi, J. High Energy Phys. **06**, 038 (2008).
[22] G. P. Salam and G. Soyez, J. High Energy Phys. **05**, 086 (2007).
[23] C. W. Bauer and B. O. Lange, arXiv:0905.4739 [hep-ph].
[24] A. D. Martin *et al.*, Eur. Phys. J. C **63**, 189 (2009).
[25] J. Pumplin *et al.*, J. High Energy Phys. **07**, 012 (2002); D. Stump *et al.*, J. High Energy Phys. **10**, 046 (2003).
[26] See the Appendix.
[27] V. M. Abazov *et al.* [D0 Collaboration], Phys. Lett. B **678**, 45 (2009).
[28] V. M. Abazov *et al.* [D0 Collaboration], Phys. Lett. B **682**, 370 (2010).

Appendix: Tables of Measurements, pQCD calculations and non-perturbative hadronization corrections

In this appendix, we provide tables of the measured differential cross sections, theory predictions and hadronization corrections described in this paper. The region that defines the kinematic phase space of the measurement at particle level is given by the electron transverse momentum, $p_T^e \geq 15$ GeV, and pseudorapidity $|\eta^e| < 1.1$, total transverse energy of all neutrinos $E_T^\nu > 20$ GeV, W transverse mass $M_T^W > 40$ GeV, jet transverse momentum $p_T^{\rm jet} \geq 20$ GeV and rapidity $|y^{\rm jet}| < 3.2$. Inclusive cross sections correspond to the sum over all $p_T^{\rm jet}$ in the given jet multiplicity, and the normalized cross sections are the absolute cross sections in a given jet multiplicity divided by the inclusive W cross sections in the kinematic region. The hadronization corrections can be applied as a multiplicative factor to parton level jets clustered using the SISCONE algorithm to produce particle jets, as defined by the D0 midpoint algorithm.

TABLE I: Measured differential cross section, normalized to the measured inclusive W cross section, as a function of leading jet p_T for events with one or more identified jets, along with statistical and systematic uncertainties.

$E_T^{\text{Leading jet}}$ (GeV)	$\langle E_T^{\text{Leading jet}} \rangle$ (GeV)	$1/\sigma_W \cdot d\sigma/dp_T^{\text{Leading jet}}$ (1/GeV)
$20-30$	24.6	$\left(5.93 \pm 0.02(\text{stat})^{+0.70}_{-0.52}(\text{syst})\right) \times 10^{-3}$
$30-40$	34.7	$\left(2.29 \pm 0.01(\text{stat})^{+0.10}_{-0.11}(\text{syst})\right) \times 10^{-3}$
$40-50$	44.7	$\left(1.130 \pm 0.006(\text{stat}) \pm 0.042(\text{syst})\right) \times 10^{-3}$
$50-60$	54.8	$\left(6.16 \pm 0.05(\text{stat}) \pm 0.26(\text{syst})\right) \times 10^{-4}$
$60-70$	64.8	$\left(3.43 \pm 0.03(\text{stat})^{+0.15}_{-0.14}(\text{syst})\right) \times 10^{-4}$
$70-80$	74.8	$\left(2.006 \pm 0.023(\text{stat})^{+0.086}_{-0.082}(\text{syst})\right) \times 10^{-4}$
$80-90$	84.8	$\left(1.227 \pm 0.016(\text{stat})^{+0.057}_{-0.053}(\text{syst})\right) \times 10^{-4}$
$90-110$	99.3	$\left(6.45 \pm 0.09(\text{stat})^{+0.36}_{-0.33}(\text{syst})\right) \times 10^{-5}$
$110-130$	119.3	$\left(2.78 \pm 0.05(\text{stat})^{+0.20}_{-0.18}(\text{syst})\right) \times 10^{-5}$
$130-150$	139.3	$\left(1.30 \pm 0.04(\text{stat})^{+0.12}_{-0.11}(\text{syst})\right) \times 10^{-5}$
$150-170$	159.2	$\left(6.50 \pm 0.25(\text{stat})^{+0.73}_{-0.64}(\text{syst})\right) \times 10^{-6}$
$170-210$	187.4	$\left(2.56 \pm 0.11(\text{stat})^{+0.32}_{-0.28}(\text{syst})\right) \times 10^{-6}$
$210-300$	241.8	$\left(4.53 \pm 0.29(\text{stat})^{+0.60}_{-0.53}(\text{syst})\right) \times 10^{-7}$
Integrated (normalized) cross section:		$0.109 \pm 0.0002(\text{stat})^{+0.007}_{-0.005}(\text{syst})$

TABLE II: Normalized NLO theory predictions for W+1 jet cross sections before application of hadronization corrections for the leading jet p_T.

$E_T^{\text{Leading jet}}$ (GeV)	$1/\sigma_W \cdot d\sigma/dp_T^{\text{Leading jet}}$ (1/GeV)	+1 standard deviation	−1 standard deviation
MCFM cross section predictions normalized by the MCFM inclusive W cross section			
20-30	5.91×10^{-3}	$+3.0 \times 10^{-4}$	-3.7×10^{-4}
30-40	2.74×10^{-3}	$+1.9 \times 10^{-4}$	-1.8×10^{-4}
40-50	1.38×10^{-3}	$+0.9 \times 10^{-4}$	-1.1×10^{-4}
50-60	7.30×10^{-4}	$+5.5 \times 10^{-5}$	-5.4×10^{-5}
60-70	4.16×10^{-4}	$+3.5 \times 10^{-5}$	-3.7×10^{-5}
70-80	2.44×10^{-4}	$+1.8 \times 10^{-5}$	-2.4×10^{-5}
80-90	1.44×10^{-4}	$+1.7 \times 10^{-5}$	-0.8×10^{-5}
90-110	7.59×10^{-5}	$+6.6 \times 10^{-6}$	-6.9×10^{-6}
110-130	3.35×10^{-5}	$+3.2 \times 10^{-6}$	-3.5×10^{-6}
130-150	1.56×10^{-5}	$+1.1 \times 10^{-6}$	-1.6×10^{-6}
150-170	7.3×10^{-6}	$+1.3 \times 10^{-6}$	-0.6×10^{-6}
170-210	3.28×10^{-6}	$+2.4 \times 10^{-7}$	-6.6×10^{-7}
210-300	5.30×10^{-7}	$+1.9 \times 10^{-8}$	-8.0×10^{-8}
BLACKHAT+SHERPA cross section predictions normalized by the BLACKHAT+SHERPA inclusive W cross section			
20-30	6.14×10^{-3}	$+1.9 \times 10^{-4}$	-3.1×10^{-4}
30-40	2.71×10^{-3}	$+1.0 \times 10^{-4}$	-1.5×10^{-4}
40-50	1.341×10^{-3}	$+4.7 \times 10^{-5}$	-7.7×10^{-5}
50-60	7.18×10^{-4}	$+2.9 \times 10^{-5}$	-4.5×10^{-5}
60-70	4.05×10^{-4}	$+2.1 \times 10^{-5}$	-2.8×10^{-5}
70-80	2.37×10^{-4}	$+1.3 \times 10^{-5}$	-1.7×10^{-5}
80-90	1.43×10^{-4}	$+0.8 \times 10^{-5}$	-1.0×10^{-5}
90-110	7.49×10^{-5}	$+5.3 \times 10^{-6}$	-6.0×10^{-6}
110-130	3.31×10^{-5}	$+2.6 \times 10^{-6}$	-2.9×10^{-6}
130-150	1.55×10^{-5}	$+1.3 \times 10^{-6}$	-1.4×10^{-6}
150-170	7.43×10^{-6}	$+6.0 \times 10^{-7}$	-6.4×10^{-7}
170-210	3.17×10^{-6}	$+3.4 \times 10^{-7}$	-3.3×10^{-7}
210-300	5.46×10^{-7}	$+5.6 \times 10^{-8}$	-6.0×10^{-8}

TABLE III: Hadronization corrections derived with SHERPA 1.2.3 and the CTEQ6.6 PDF set for the leading jet p_T distribution.

$E_T^{\text{Leading jet}}$ (GeV)	Hadronization correction
20-30	1.110 ± 0.004
30-40	0.968 ± 0.005
40-50	0.907 ± 0.005
50-60	0.914 ± 0.007
60-70	0.892 ± 0.008
70-80	0.898 ± 0.009
80-90	0.87 ± 0.01
90-110	0.869 ± 0.01
110-130	0.85 ± 0.01
130-150	0.85 ± 0.015
150-170	0.82 ± 0.02
170-210	0.79 ± 0.02
210-300	0.74 ± 0.03

TABLE IV: Measured differential cross section, normalized to the measured inclusive W cross section, as a function of second jet p_T for events with two or more identified jets, along with statistical and systematic uncertainties.

$E_T^{\text{Second jet}}$ (GeV)	$\langle E_T^{\text{Second jet}} \rangle$ (GeV)	$1/\sigma_W \cdot d\sigma/dp_T^{\text{Second jet}}$ (1/GeV)
$20-30$	24.4	$\left(1.10 \pm 0.01(\text{stat})^{+0.19}_{-0.13}(\text{syst})\right) \times 10^{-3}$
$30-40$	34.6	$\left(3.36 \pm 0.03(\text{stat})^{+0.36}_{-0.30}(\text{syst})\right) \times 10^{-4}$
$40-50$	44.7	$\left(1.38 \pm 0.019(\text{stat})^{+0.093}_{-0.090}(\text{syst})\right) \times 10^{-4}$
$50-60$	54.7	$\left(6.51 \pm 0.12(\text{stat}) \pm 0.37(\text{syst})\right) \times 10^{-5}$
$60-70$	64.7	$\left(3.33 \pm 0.09(\text{stat})^{+0.19}_{-0.18}(\text{syst})\right) \times 10^{-5}$
$70-80$	74.8	$\left(1.84 \pm 0.06(\text{stat})^{+0.11}_{-0.10}(\text{syst})\right) \times 10^{-5}$
$80-100$	89.0	$\left(8.52 \pm 0.3(\text{stat})^{+0.52}_{-0.50}(\text{syst})\right) \times 10^{-6}$
$100-140$	117.1	$\left(2.38 \pm 0.11(\text{stat})^{+0.15}_{-0.14}(\text{syst})\right) \times 10^{-6}$
$140-180$	155.8	$\left(5.16 \pm 0.51(\text{stat})^{+0.40}_{-0.37}(\text{syst})\right) \times 10^{-7}$
$180-250$	199.3	$\left(9.4 \pm 1.6(\text{stat})^{+1.3}_{-1.3}(\text{syst})\right) \times 10^{-8}$
Integrated (normalized) cross section:		$0.017 \pm 0.0001(\text{stat})^{+2.0\times10^{-3}}_{-1.4\times10^{-3}}(\text{syst})$

TABLE V: Normalized NLO theory predictions for W+2 jet cross sections before application of hadronization corrections for the second jet p_T.

$E_T^{\text{Second jet}}$ (GeV)	$1/\sigma_W \cdot d\sigma/dp_T^{\text{Second jet}}$ (1/GeV)	+1 standard deviation	−1 standard deviation
MCFM cross section predictions normalized by the MCFM inclusive W cross section			
20-30	9.01×10^{-4}	+0.0	-6.4×10^{-5}
30-40	2.97×10^{-4}	+0.0	-1.6×10^{-5}
40-50	1.19×10^{-4}	+0.0	-1.1×10^{-5}
50-60	5.44×10^{-5}	+0.0	-6.2×10^{-6}
60-70	2.81×10^{-5}	+0.0	-2.2×10^{-6}
70-80	1.54×10^{-5}	+0.0	-2.1×10^{-6}
80-100	7.50×10^{-6}	+0.0	-9.5×10^{-7}
100-140	2.11×10^{-6}	+0.0	-4.2×10^{-7}
140-180	4.56×10^{-7}	+0.0	-4.6×10^{-8}
180-250	8.29×10^{-8}	+0.0	-9.1×10^{-9}
BLACKHAT+SHERPA cross section predictions normalized by the BLACKHAT+SHERPA inclusive W cross section			
20-30	1.17×10^{-3}	$+0.7 \times 10^{-4}$	-1.3×10^{-4}
30-40	3.73×10^{-4}	$+2.1 \times 10^{-5}$	-4.1×10^{-5}
40-50	1.48×10^{-4}	$+0.7 \times 10^{-5}$	-1.5×10^{-5}
50-60	7.10×10^{-5}	$+3.9 \times 10^{-6}$	-7.6×10^{-6}
60-70	3.57×10^{-5}	$+1.2 \times 10^{-6}$	-3.5×10^{-6}
70-80	1.96×10^{-5}	$+0.8 \times 10^{-6}$	-1.8×10^{-6}
80-100	9.38×10^{-6}	$+3.5 \times 10^{-7}$	-9.1×10^{-7}
100-140	2.60×10^{-6}	$+0.4 \times 10^{-7}$	-2.2×10^{-7}
140-180	5.47×10^{-7}	+0.0	-4.6×10^{-8}
180-250	1.03×10^{-7}	+0.0	-1.0×10^{-8}

TABLE VI: Hadronization corrections derived with SHERPA 1.2.3 and CTEQ6.6 PDF set for the second jet p_T distribution.

$E_T^{\text{Second jet}}$ (GeV)	Hadronization correction
20-30	1.133 ± 0.006
30-40	0.942 ± 0.009
40-50	0.89 ± 0.01
50-60	0.92 ± 0.02
60-70	0.88 ± 0.02
70-80	0.82 ± 0.03
80-100	0.85 ± 0.03
100-140	0.88 ± 0.03
140-180	0.85 ± 0.05
180-250	0.62 ± 0.05

TABLE VII: Measured differential cross section, normalized to the measured inclusive W cross section, as a function of third jet p_T for events with three or more identified jets, along with statistical and systematic uncertainties.

$E_T^{\text{Third jet}}$ (GeV)	$\langle E_T^{\text{Third jet}} \rangle$ (GeV)	$1/\sigma_W \cdot d\sigma/dp_T^{\text{Third jet}}$ (1/GeV)
$20-30$	24.3	$\left(1.99 \pm 0.04(\text{stat})^{+0.35}_{-0.28}(\text{syst})\right) \times 10^{-4}$
$30-50$	38.1	$\left(2.87 \pm 0.10(\text{stat})^{+0.26}_{-0.27}(\text{syst})\right) \times 10^{-5}$
$50-80$	61.8	$\left(2.53 \pm 0.20(\text{stat})^{+0.34}_{-0.39}(\text{syst})\right) \times 10^{-6}$
$80-130$	96.2	$\left(1.47 \pm 0.26(\text{stat})^{+0.24}_{-0.25}(\text{syst})\right) \times 10^{-7}$
Integrated (normalized) cross section:		$0.0026 \pm 0.5 \times 10^{-4}(\text{stat})^{+3.6\times10^{-4}}_{-2.9\times10^{-4}}(\text{syst})$

TABLE VIII: Normalized NLO theory predictions before application of hadronization corrections for third jet p_T.

$E_T^{\text{Third jet}}$ (GeV)	$1/\sigma_W \cdot d\sigma/dp_T^{\text{Third jet}}$ (1/GeV)	+1 standard deviation	−1 standard deviation
ROCKET+MCFM cross section predictions normalized by the ROCKET+MCFM inclusive W cross section			
20-30	1.545×10^{-4}	$+5.1 \times 10^{-6}$	-2.7×10^{-5}
30-50	2.38×10^{-5}	$+0.8 \times 10^{-6}$	-4.1×10^{-6}
50-80	2.01×10^{-6}	$+0.9 \times 10^{-7}$	-3.5×10^{-7}
80-130	1.16×10^{-7}	$+1.5 \times 10^{-8}$	-1.6×10^{-8}
BLACKHAT+SHERPA cross section predictions normalized by the BLACKHAT+SHERPA inclusive W cross section			
20-30	1.84×10^{-4}	$+2.1 \times 10^{-5}$	-3.2×10^{-5}
30-50	2.63×10^{-5}	$+3.0 \times 10^{-6}$	-4.3×10^{-6}
50-80	2.23×10^{-6}	$+2.4 \times 10^{-7}$	-3.6×10^{-7}
80-130	1.29×10^{-7}	$+1.2 \times 10^{-8}$	-2.1×10^{-8}

TABLE IX: Hadronization corrections derived with SHERPA 1.2.3 and the CTEQ6.6 PDF set for the third jet p_T distribution.

$E_T^{\text{Third jet}}$ (GeV)	Hadronization correction
20-30	1.092 ± 0.010
30-50	0.866 ± 0.009
50-80	0.83 ± 0.02
80-130	0.75 ± 0.03

TABLE X: Measured differential cross section, normalized to the measured inclusive W cross section, as a function of fourth jet p_T for events with four or more identified jets, along with statistical and systematic uncertainties.

$E_T^{\text{Fourth jet}}$ (GeV)	$\langle E_T^{\text{Fourth jet}} \rangle$ (GeV)	$1/\sigma_W \cdot d\sigma/dp_T^{\text{Fourth jet}}$ (1/GeV)
$20-30$	24.1	$\left(2.97 \pm 0.17(\text{stat})^{+0.75}_{-0.55}(\text{syst})\right) \times 10^{-5}$
$30-50$	37.6	$\left(2.44 \pm 0.31(\text{stat})^{+0.59}_{-0.57}(\text{syst})\right) \times 10^{-6}$
$50-80$	60.3	$\left(9.8 \pm 2.8(\text{stat})^{+9.4}_{-8.7}(\text{syst})\right) \times 10^{-8}$
Integrated (normalized) cross section:		$0.00035 \pm 1.8 \times 10^{-5}(\text{stat})^{+7.6\times10^{-5}}_{-5.6\times10^{-5}}(\text{syst})$

TABLE XI: Normalized LO theory predictions before application of hadronization corrections for fourth jet p_T.

$E_T^{\text{Fourth jet}}$ (GeV)	$1/\sigma_W \cdot d\sigma/dp_T^{\text{Fourth jet}}$ (1/GeV)	+1 standard deviation	−1 standard deviation
ROCKET+MCFM cross section predictions normalized by the ROCKET+MCFM inclusive W cross section			
20-30	2.9×10^{-5}	$+2.5 \times 10^{-5}$	-1.2×10^{-5}
30-50	2.7×10^{-6}	$+2.3 \times 10^{-6}$	-1.1×10^{-6}
50-80	1.22×10^{-7}	$+1.1 \times 10^{-7}$	-5.4×10^{-8}
BLACKHAT+SHERPA cross section predictions normalized by the BLACKHAT+SHERPA inclusive W cross section			
20-30	3.0×10^{-5}	$+2.5 \times 10^{-5}$	-1.2×10^{-5}
30-50	2.7×10^{-6}	$+2.3 \times 10^{-6}$	-1.1×10^{-6}
50-80	1.18×10^{-7}	$+9.8 \times 10^{-8}$	-4.7×10^{-8}

TABLE XII: Hadronization corrections derived with SHERPA 1.2.3 and the CTEQ6.6 PDF set for the fourth jet p_T distribution.

$E_T^{\text{Fourth jet}}$ (GeV)	Hadronization correction
20-30	1.120 ± 0.018
30-50	0.863 ± 0.016
50-80	0.741 ± 0.027

TABLE XIII: Measurement of n^{th} jet inclusive cross section in association with a W boson. All results are given in pb.

Bin	$\sigma_{W+\text{n-jet}}$ (pb)	Statistical Uncertainty (pb)	Systematic Uncertainty (pb)
$W+0$-jet	1132	$\pm$ 0.8 (stat)	$^{+81}_{-92}$ (syst)
$W+1$-jet	123.1	$\pm$ 0.3 (stat)	$^{+9.6}_{-8.5}$ (syst)
$W+2$-jet	19.5	$\pm$ 0.1 (stat)	$^{+2.4}_{-1.9}$ (syst)
$W+3$-jet	3.0	$\pm$ 0.1 (stat)	$^{+0.4}_{-0.4}$ (syst)
$W+4$-jet	0.40	$\pm$ 0.02 (stat)	$^{+0.09}_{-0.07}$ (syst)

TABLE XIV: Measurement of n^{th} jet to $(n-1)^{\text{th}}$ jet inclusive cross section ratios.

σ_n/σ_{n-1}	Ratio (data)
σ_1/σ_0	$0.109^{+0.007}_{-0.005}$
σ_2/σ_1	$0.158^{+0.009}_{-0.006}$
σ_3/σ_2	$0.154^{+0.007}_{-0.007}$
σ_4/σ_3	$0.133^{+0.015}_{-0.010}$

TABLE XV: BLACKHAT+SHERPA and ROCKET+MCFM predictions of n^{th} jet to $(n-1)^{\text{th}}$ jet inclusive cross section ratios before hadronization corrections.

σ_n/σ_{n-1}	Ratio (BLACKHAT+SHERPA, no hadronization correction)
σ_1/σ_0	$0.120^{+0.004}_{-0.007}$
σ_2/σ_1	$0.155^{+0.003}_{-0.009}$
σ_3/σ_2	$0.131^{+0.007}_{-0.009}$
σ_4/σ_3	$0.11^{+0.02}_{-0.01}$
σ_n/σ_{n-1}	Ratio (ROCKET+MCFM, no hadronization correction)
σ_1/σ_0	$0.119^{+0.008}_{-0.008}$
σ_2/σ_1	$0.122^{+0.0004}_{-0.014}$
σ_3/σ_2	$0.145^{+0.014}_{-0.017}$
σ_4/σ_3	$0.13^{+0.02}_{-0.01}$

TABLE XVI: Inclusive hadronization correction derived with SHERPA 1.2.3 and the CTEQ6.6 PDF set for each inclusive jet bin.

Inclusive jet multiplicity bin	Inclusive hadronization correction
0-jet	1.00
1-jet	1.06
2-jet	1.10
3-jet	1.11
4-jet	1.16